

RECEIVED: August 9, 2024

REVISED: October 22, 2024

ACCEPTED: November 2, 2024

PUBLISHED: November 21, 2024

Search for the radiative decay $D_s^+ \rightarrow \gamma\rho(770)^+$

The BESIII collaboration

E-mail: besiii-publications@ihep.ac.cn

ABSTRACT: Using 7.33 fb^{-1} of e^+e^- collision data samples collected with the BESIII detector at center-of-mass energies between 4.128 and 4.226 GeV, we search for the radiative decay $D_s^+ \rightarrow \gamma\rho(770)^+$ for the first time. A hint of $D_s^+ \rightarrow \gamma\rho(770)^+$ is observed with a statistical significance of 2.5σ . The branching fraction of $D_s^+ \rightarrow \gamma\rho(770)^+$ is measured to be $(2.2 \pm 0.9_{\text{stat.}} \pm 0.2_{\text{syst.}}) \times 10^{-4}$, corresponding to an upper limit of 6.1×10^{-4} at the 90% confidence level.

KEYWORDS: Branching fraction, Charm Physics, e^+e^- Experiments, Rare Decay

ARXIV EPRINT: [2408.03980](https://arxiv.org/abs/2408.03980)

Contents

1	Introduction	1
2	Detector and data sets	2
3	Analysis strategy	3
4	Event selection	3
5	Branching fraction measurement	7
6	Systematic uncertainty	9
7	Summary	11
	The BESIII collaboration	16

1 Introduction

In the rare radiative decays of charmed mesons, it has been established that the short-distance interactions of the $c \rightarrow u\gamma$ process make a negligible contribution [1, 2]. Consequently, long-distance, non-perturbative processes dominate these decays, potentially enhancing branching fractions (BFs) up to 10^{-3} [3–7]. Therefore, measurements of BFs of these decays can be used to test the quantum chromodynamics (QCD)-based calculations of long-distance dynamics [8, 9]. Theoretical physicists have conducted analyses on the CP asymmetry of $D_s^+ \rightarrow \gamma\rho(770)^+$ considering the matrix element contributions of the \mathcal{O}_8 operator in the rare decay Hamiltonian [10]. The BF of $D_s^+ \rightarrow \gamma\rho(770)^+$ can be used to examine the predictions regarding CP asymmetry in charmed meson decays.

Recent experimental results on rare radiative charm decays offer a chance to improve the theoretical understanding of physics involved in the $c \rightarrow u\gamma$ transition [11]. However, to date, there have been no experimental results for rare radiative decays of D_s^+ mesons, such as the Cabibbo-favored decay $D_s^+ \rightarrow \gamma\rho(770)^+$. The BF of this mode is expected to lie within the range of $\mathcal{O}(10^{-5}) - \mathcal{O}(10^{-3})$, according to the predictions of different models like QCD sum rules [12], light-cone sum rules [10], the vector-meson dominance [1], the hybrid framework [4, 6] and weak annihilation [13]. The predictions of the various theoretical calculations are quite divergent for the decay mode $D_s^+ \rightarrow \gamma\rho(770)^+$, which underlines the urgent need for experimental results to discriminate among different models.

In this paper, we search for the radiative decay $D_s^+ \rightarrow \gamma\rho(770)^+$ for the first time, using 7.33 fb^{-1} data collected with the BESIII detector in e^+e^- collision center of-mass energies (E_{cm}) between 4.128 and 4.226 GeV, where E_{cm} is the energy of the initial state calculated from the beam energy in the e^+e^- center-of-mass frame.

E_{cm} (GeV) [20, 21]	\mathcal{L}_{int} (pb ⁻¹) [22]	M_{rec} (GeV/ c^2)
4.128	401.5	[2.060, 2.150]
4.157	408.7	[2.054, 2.170]
4.178	3189.0 ± 0.2 ± 31.9	[2.050, 2.180]
4.189	570.0 ± 0.1 ± 2.2	[2.048, 2.190]
4.199	526.0 ± 0.1 ± 2.1	[2.046, 2.200]
4.209	572.1 ± 0.1 ± 1.8	[2.044, 2.210]
4.219	569.2 ± 0.1 ± 1.8	[2.042, 2.220]
4.226	1100.9 ± 0.1 ± 7.0	[2.040, 2.220]

Table 1. The integrated luminosities (\mathcal{L}_{int}) and the requirements on the D_s^- recoil mass (M_{rec}) for various center-of-mass energies. The definition of M_{rec} is given in eq. (4.1). The first and second uncertainties for \mathcal{L} are statistical and systematic, respectively. The integrated luminosities for the two data samples at $E_{\text{cm}} = 4.128$ GeV and $E_{\text{cm}} = 4.157$ GeV are estimated by using online monitoring information.

2 Detector and data sets

The BESIII detector records symmetric e^+e^- collisions provided by the BEPCII storage ring [14], in the center-of-mass energy range from 2.0 to 4.95 GeV, with a peak luminosity of $1.1 \times 10^{33} \text{ cm}^{-2}\text{s}^{-1}$ achieved at the center-of-mass energy of 3.773 GeV. The cylindrical core of the BESIII detector covers 93% of the full solid angle and consists of a helium-based multilayer drift chamber (MDC), a plastic scintillator time-of-flight system (TOF), and a CsI(Tl) electromagnetic calorimeter (EMC), which are all enclosed in a superconducting solenoidal magnet providing a 1.0 T magnetic field. The solenoid is supported by an octagonal flux-return yoke with resistive plate counter muon identification modules interleaved with steel. The charged-particle momentum resolution at 1 GeV/ c is 0.5%, and the dE/dX resolution is 6% for electrons from Bhabha scattering. The EMC measures photon energies with a resolution of 2.5% (5%) at 1 GeV in the barrel (end-cap) region. The time resolution in the TOF barrel region is 68 ps, while that in the end-cap region is 110 ps. The end-cap TOF system was upgraded in 2015 using multi-gap resistive plate chamber technology, providing a time resolution of 60 ps [15–17]. About 83% of the data in this analysis benefits from the upgrade.

The data samples are organized into four groups, $E_{\text{cm}} = 4.128$ and 4.157 GeV (I), 4.178 GeV (II), four energies from 4.189 to 4.219 GeV (III), and 4.226 GeV (IV), that were acquired during the same year under consistent running conditions. The integrated luminosities at each energy is given in table 1. At these energies, the cross section of $D_s^{*\pm}D_s^\mp$ production in e^+e^- annihilation is about a factor of twenty larger than that of $D_s^\pm D_s^\mp$ [18, 19]. To increase the sensitivity of this search, the events discussed in this paper are selected from the process $e^+e^- \rightarrow D_s^{*\pm}D_s^\mp$.

Inclusive Monte Carlo (MC) samples, which are 40 times larger than the data sets, are produced in the energy range $E_{\text{cm}} = 4.128$ to 4.226 GeV with a GEANT4-based [23] software package, which includes the geometric description of the BESIII detector and the

detector response. These samples are used to determine the detection efficiencies and estimate backgrounds. The samples include the production of open charm processes, the initial-state radiation production of vector charmonium(-like) states and the continuum processes incorporated in KKMC [24, 25]. All particle decays are modeled with EVTGEN [26, 27] using BFs either reported by the PDG [28], when available, or otherwise estimated with LUNDCHARM [29, 30]. Final state radiation from charged particles is incorporated using PHOTOS [31]. For the signal Monte Carlo samples, we generate 3.2 million events for the decay $D_s^+ \rightarrow \gamma\rho(770)^+$, $\rho(770)^+ \rightarrow \pi^0\pi^+$, and $\pi^0 \rightarrow \gamma\gamma$. The $D_s^+ \rightarrow \gamma\rho(770)^+$ decay is parameterized by helicity amplitudes [7–9], resulting in an angular distribution of $1 - \cos^2\theta_H$, in which θ_H is the helicity angle between the momentum vector of the particle π^+ in the $\rho(770)^+$ rest frame and the direction of the $\rho(770)^+$ system in the D_s^+ rest frame. The decay $\rho(770)^+ \rightarrow \pi^0\pi^+$ is modeled with VSS [26, 27], which describes the decay of a vector meson to scalar-scalar mesons. The decay $\pi^0 \rightarrow \gamma\gamma$ is generated with a uniform phase-space model [24, 25].

3 Analysis strategy

The $D_s^{*\pm}D_s^\mp \rightarrow \gamma(\pi^0)D_s^\pm D_s^\mp$ pairs are produced by e^+e^- collisions in the energy range of 4.128 to 4.226 GeV. This property enables the study of D_s^+ decays utilizing the double-tag (DT) method, which was pioneered by the MARK-III collaboration [32]. At first, single-tag (ST) D_s^- candidates are selected by reconstructing a D_s^- in five hadronic decay modes: $D_s^- \rightarrow K_S^0 K^-$, $D_s^- \rightarrow K^+ K^- \pi^-$, $D_s^- \rightarrow K^+ K^- \pi^- \pi^0$, $D_s^- \rightarrow K_S^0 K^+ \pi^- \pi^-$ and $D_s^- \rightarrow K^- \pi^- \pi^+$, based on the optimization of the figure of merit $S/\sqrt{(S+B)}$. Here, S is the signal yield expected based on the predicted BF of $D_s^+ \rightarrow \gamma\rho(770)^+$ [10] and B is the scaled background yield estimated by the inclusive MC sample. Events in which a signal candidate is reconstructed in the presence of an ST D_s^- meson are denoted as DT events.

The BF of the signal decay is determined by

$$\mathcal{B}(D_s^+ \rightarrow \gamma\rho(770)^+) = \frac{N_{\text{total}}^{\text{DT}}}{B(\pi^0 \rightarrow \gamma\gamma) \sum_{\alpha,i} N_{\alpha,i}^{\text{ST}} \epsilon_{\alpha,i}^{\text{DT}} / \epsilon_{\alpha,i}^{\text{ST}}}, \quad (3.1)$$

where $\mathcal{B}(\pi^0 \rightarrow \gamma\gamma)$ is the BF of $\pi^0 \rightarrow \gamma\gamma$ in the $\rho^+ \rightarrow \pi^+\pi^0$ decay. $N_{\text{total}}^{\text{DT}}$ is the summed number of the DT yields for all four sample groups. $\epsilon_{\alpha,i}^{\text{ST}}$ is the ST efficiency to reconstruct the ST mode i in the sample group α , and $\epsilon_{\alpha,i}^{\text{DT}}$ is the DT efficiency for reconstructing the ST mode i and the signal decay mode in the sample group α . Charge-conjugated modes are implicitly considered throughout this paper.

4 Event selection

Charged tracks detected in the MDC are required to be within a polar angle (θ) range of $|\cos\theta| < 0.93$, where θ is defined with respect to the z -axis, which is the symmetry axis of the MDC. For charged tracks not originating from K_S^0 decays, the distance of closest approach to the interaction point (IP) is required to be less than 10 cm along the z -axis, $|V_z|$, and less than 1 cm in the transverse plane, $|V_{xy}|$. Particle identification (PID) for charged tracks combines the measurements of dE/dx in the MDC and the time of flight in

Tag mode	Mass window (GeV/ c^2)
$D_s^- \rightarrow K_S^0 K^-$	[1.948, 1.991]
$D_s^- \rightarrow K^+ K^- \pi^-$	[1.950, 1.986]
$D_s^- \rightarrow K^+ K^- \pi^- \pi^0$	[1.947, 1.982]
$D_s^- \rightarrow K_S^0 K^+ \pi^- \pi^-$	[1.953, 1.983]
$D_s^- \rightarrow K^- \pi^- \pi^+$	[1.953, 1.983]

Table 2. Requirements on M_{tag} for various tag modes.

the TOF to form likelihoods $\mathcal{L}(h)$ ($h = K, \pi$) for each hadron hypothesis. Charged kaons and pions are identified by comparing the likelihoods for the two hypotheses, $\mathcal{L}(K) > \mathcal{L}(\pi)$ and $\mathcal{L}(\pi) > \mathcal{L}(K)$, respectively.

K_S^0 candidates are reconstructed with two oppositely charged tracks that satisfy $|V_z| < 20$ cm, assigned as $\pi^+\pi^-$ and without PID imposed. Primary vertex and secondary vertex fits are performed on these two charged tracks with $\pi^+\pi^-$ hypothesis to determine the invariant mass and the decay length of K_S^0 candidates. The K_S^0 candidates are required to have a $\pi^+\pi^-$ invariant mass ($M_{\pi^+\pi^-}$) within [0.487, 0.511] GeV/ c^2 , and the decay length to be larger than twice its resolution. This requirement is not applied for the $D_s^- \rightarrow K_S^0 K^-$ decay due to the low combinatorial background. To avoid double-counting an event in both the $D_s^- \rightarrow K_S^0 K^-$ and $D_s^- \rightarrow K^- \pi^- \pi^+$ ST modes, $M_{\pi^+\pi^-}$ is required to be outside the mass range [0.487, 0.511] GeV/ c^2 for the $D_s^- \rightarrow K^- \pi^- \pi^+$ mode.

Photon candidates are identified using showers in the EMC. The deposited energy of each shower must be more than 25 MeV in the barrel region ($|\cos\theta| < 0.80$) and more than 50 MeV in the end-cap region ($0.86 < |\cos\theta| < 0.92$). To exclude showers that originate from charged tracks, the opening angle subtended by the EMC shower and the position of the closest charged track at the EMC must be greater than 10° as measured from the IP. The difference between the EMC time and the event start time is required to be within [0, 700] ns to suppress electronic noise and showers unrelated to the event.

π^0 candidates are reconstructed through the $\pi^0 \rightarrow \gamma\gamma$ decay, with at least one photon being detected in the barrel region. The invariant mass of the photon pair must be in the range of [0.115, 0.150] GeV/ c^2 , approximately three times the mass resolution around the known π^0 mass [28]. A kinematic fit is performed that constrains the $\gamma\gamma$ invariant mass to the known π^0 mass to improve the mass resolution and the χ^2 is required to be less than 30.

Five ST modes are used for the reconstruction of D_s^- candidates, with corresponding mass windows on the tagging invariant D_s^- mass (M_{tag}) determined through fits as listed in table 2. The recoiling mass (M_{rec}) against the tagging D_s^- is evaluated, and events with M_{rec} within the mass windows specified in table 1 are retained for further analysis. These M_{rec} ranges are chosen by maintaining roughly constant the tag efficiencies for different values of E_{cm} . The recoiling mass M_{rec} is defined as

$$M_{\text{rec}} = \sqrt{\left(E_{\text{cm}}/c^2 - \sqrt{|\vec{p}_{D_s^-}/c|^2 + m_{D_s^-}^2}\right)^2 - |\vec{p}_{D_s^-}/c|^2}, \quad (4.1)$$

Tag mode	N_{I}^{ST}	$N_{\text{II}}^{\text{ST}}$	$N_{\text{III}}^{\text{ST}}$	$N_{\text{IV}}^{\text{ST}}$
$D_s^- \rightarrow K_S^0 K^-$	6728 ± 144	31949 ± 314	19960 ± 270	6837 ± 163
$D_s^- \rightarrow K^+ K^- \pi^-$	27670 ± 280	137138 ± 614	86918 ± 525	29544 ± 335
$D_s^- \rightarrow K^+ K^- \pi^- \pi^0$	7457 ± 397	39340 ± 798	24694 ± 688	8084 ± 481
$D_s^- \rightarrow K_S^0 K^+ \pi^- \pi^-$	2983 ± 129	15705 ± 288	9783 ± 247	3380 ± 174
$D_s^- \rightarrow K^- \pi^- \pi^+$	3804 ± 345	17439 ± 565	10841 ± 470	5144 ± 447

Table 3. The ST yields (N_{α}^{ST}) for the data samples collected at $E_{\text{cm}} = 4.128$ and 4.157 GeV (I), 4.178 GeV (II), from 4.189 to 4.219 GeV (III), 4.226 GeV (IV). The uncertainties are statistical.

Tag mode	$\epsilon_{\text{I}}^{\text{ST}}(\%)$	$\epsilon_{\text{II}}^{\text{ST}}(\%)$	$\epsilon_{\text{III}}^{\text{ST}}(\%)$	$\epsilon_{\text{IV}}^{\text{ST}}(\%)$
$D_s^- \rightarrow K_S^0 K^-$	47.64 ± 0.16	47.39 ± 0.07	47.23 ± 0.09	47.95 ± 0.16
$D_s^- \rightarrow K^+ K^- \pi^-$	40.37 ± 0.07	39.47 ± 0.03	39.33 ± 0.04	39.78 ± 0.07
$D_s^- \rightarrow K^+ K^- \pi^- \pi^0$	10.59 ± 0.08	10.68 ± 0.03	10.74 ± 0.05	10.89 ± 0.09
$D_s^- \rightarrow K_S^0 K^+ \pi^- \pi^-$	21.30 ± 0.14	21.85 ± 0.06	21.66 ± 0.08	22.27 ± 0.16
$D_s^- \rightarrow K^- \pi^- \pi^+$	48.37 ± 0.59	47.93 ± 0.25	47.63 ± 0.34	47.67 ± 0.67

Table 4. The ST efficiencies ($\epsilon_{\alpha}^{\text{ST}}$) for the data samples collected at $E_{\text{cm}} = 4.128$ and 4.157 GeV (I), 4.178 GeV (II), from 4.189 to 4.219 GeV (III), 4.226 GeV (IV). The uncertainties are statistical.

where $\vec{p}_{D_s^-}$ is the three-momentum of the D_s^- candidate in the e^+e^- center-of-mass frame, and $m_{D_s^-}$ is the known D_s^- mass [28].

In order to remove soft pions from D^{*+} decays, the momentum requirement of $p(\pi) > 100$ MeV/ c is applied to all pions. In events with multiple ST candidates, the candidate with M_{rec} closest to the known D_s^{*+} mass [28] is chosen as the best candidate. It is observed that approximately 4.1%(4.3%) of events in data (inclusive MC) contain multiple candidates in the ST samples. The yields for the five ST modes are listed in table 3, and they are obtained through binned maximum likelihoods fits to the corresponding invariant mass distributions of ST candidates (M_{tag}). As an example, the fits to the accepted ST candidates from the data sample at $E_{\text{cm}} = 4.178$ GeV are shown in figure 1. In the fits, the signal is modeled by an MC-simulated shape convolved with a Gaussian function that accounts for the data-MC difference. The background is described by a second-order Chebyshev polynomial. For the tag mode $D_s^- \rightarrow K_S^0 K^-$, the peaking background originating from $D^- \rightarrow K_S^0 \pi^-$ is considered. The shape of this background is taken from the inclusive MC samples and included in the fit with a free yield parameter. The same ST selection criteria and fitting approach applied to data are used to analyze the inclusive MC samples. The number of observed ST events is extracted from fitting the M_{tag} distributions. The ST efficiency is calculated as the ratio of the observed ST events and the generated ST events in the inclusive MC samples, as shown in table 4. When obtaining the ST efficiencies within a grouped dataset (I and III), the yields at different energy points are averaged based on their luminosity and cross sections.

In events with a ST D_s^- candidate, we search for the $D_s^+ \rightarrow \gamma \rho(770)^+$ signal process recoiling against the ST side, with the $\rho(770)^+$ reconstructed with the $\pi^+ \pi^0$ final states. The

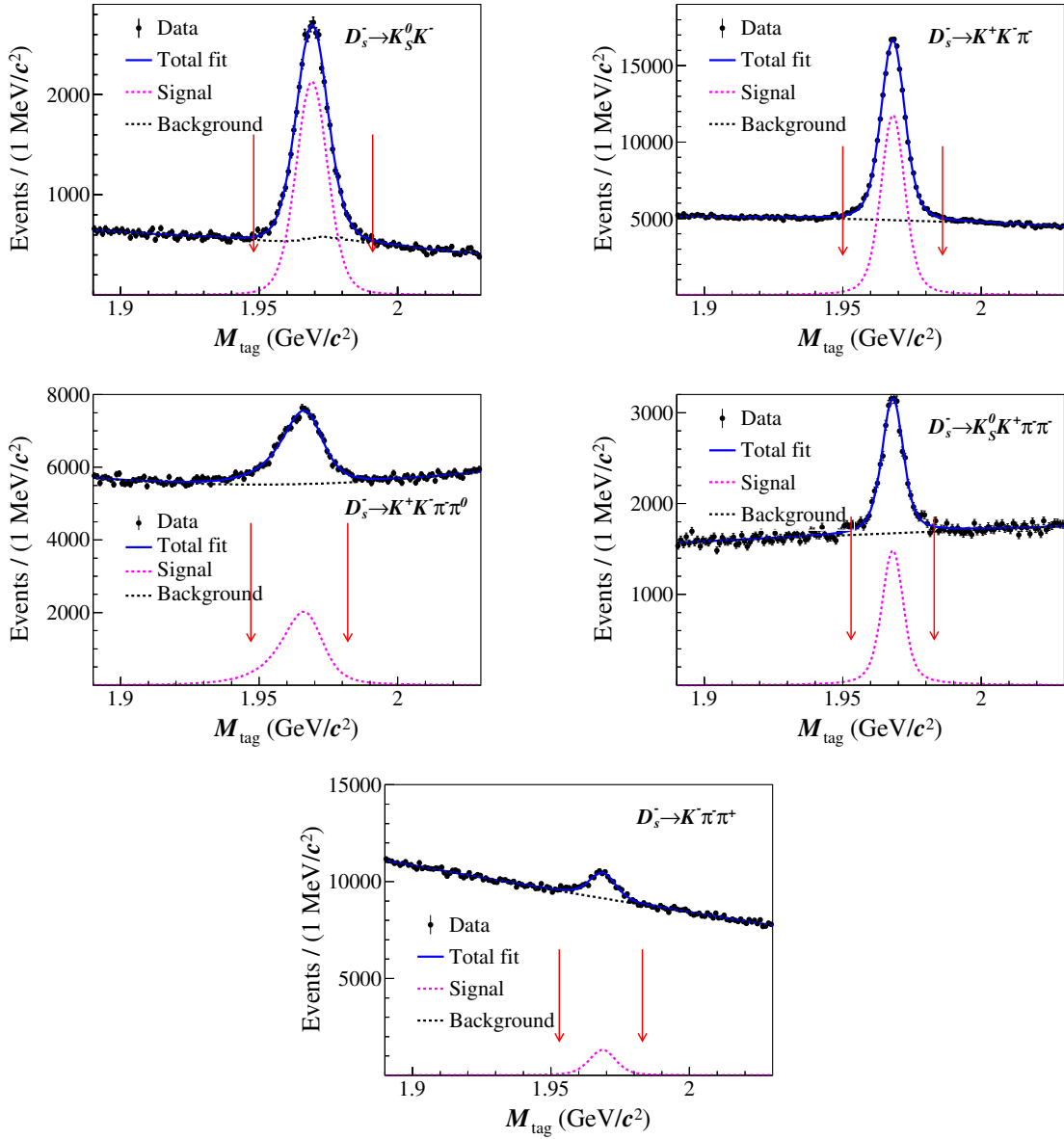


Figure 1. Fits to the M_{tag} distributions of the ST candidates from the data sample at $E_{\text{cm}} = 4.178$ GeV. The black points with error bars are data, the blue solid lines are the total fit results, the magenta dashed lines show the signal component and the black dashed lines show the background component. The pairs of red arrows denote the signal regions.

γ , π^\pm and π^0 are selected with the same criteria used in section 4. The most energetic γ not used in the tag side is used as the radiative photon. In the case of multiple candidates, the DT candidate with the average mass, $(M_{\text{sig}} + M_{\text{tag}})/2$, closest to the known D_s^\pm mass is retained, where M_{sig} represents the invariant mass of the accepted signal D_s^+ . For all ST modes, the average ratio of correct selection for multiple signal candidates is found to be 94%.

To suppress background events from $D_s^+ \rightarrow \pi^+ \eta$, $\eta \rightarrow \gamma\gamma$, a requirement of $M_{\gamma\gamma_{\text{h}}} > 0.68$ GeV/ c^2 is imposed to ensure the invariant mass is above the η invariant mass, where γ_{h} is

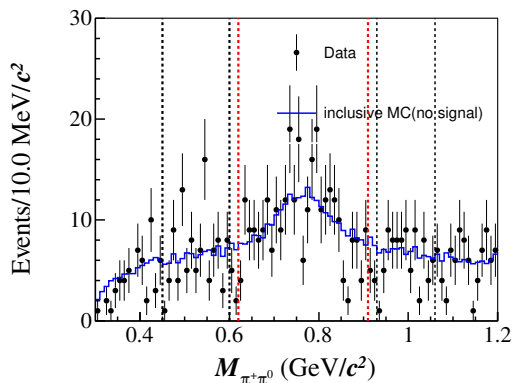


Figure 2. Invariant mass distribution for selected $\rho(770)^+ \rightarrow \pi^+\pi^0$ candidates at $\sqrt{s} = 4.128 - 4.226$ GeV. The black points with error bars are data. The solid blue line represents the inclusive MC sample, which contains no signal and has been normalized to the data. The red vertical dashed lines indicate the $\rho(770)^+$ signal region, and the pairs of black dashed lines (left and right of the signal peak) indicate the $\rho(770)^+$ sideband regions.

the photon with higher energy from the π^0 of the ρ^+ decay in the signal reaction and γ is the radiative photon from the signal process $D_s^+ \rightarrow \gamma\rho^+$. If the invariant mass of $M_{\gamma\gamma_{\text{extra}}}$ falls within the π^0 mass window $[0.115, 0.150]$ GeV/ c^2 or the η mass window $[0.50, 0.57]$ GeV/ c^2 , such candidates are vetoed, with γ_{extra} denoting an extra photon not utilized in either the ST or DT sides. The invariant mass distribution of $\pi^+\pi^0$ for data and inclusive MC sample is shown in figure 2. The mass range used for the ρ , between 0.62 and 0.91 GeV/ c^2 keeps 81% of signal events according to the simulation. Mass ranges for sideband regions which correspond to $[0.45, 0.60]$ and $[0.93, 1.06]$ GeV/ c^2 are expected to contain only 19% of signal events. These selection criteria are optimized using the figure of merit (FOM) approach, defined as $\frac{\epsilon}{1.5+\sqrt{B}}$ [33]. Here, ϵ and B denote the signal efficiency estimated by the signal MC samples and the background yields estimated by the inclusive MC samples, respectively.

5 Branching fraction measurement

After imposing all above selection criteria, the comparisons of the $M_{D_s^+}$ and $\cos\theta_H$ distributions between data and inclusive MC sample are shown in figure 3. The shapes of the inclusive MC samples demonstrate consistency with the data. The distributions of the invariant mass (M_{sig}) of signal D_s^+ candidates versus $\cos\theta_H$, M_{sig} and $\cos\theta_H$ are shown in the figures 4 (a), (b), and (c), respectively. The signal yield is extracted from a two-dimensional (2D) unbinned maximum likelihood fit on the M_{sig} versus $\cos\theta_H$ distribution for $D_s^+ \rightarrow \gamma\rho(770)^+$. The signal shape is described by an MC-simulated 2D probability density function (PDF) convolved with a 2D Gaussian function, with the parameters obtained from the control sample $D_s^+ \rightarrow \pi^+\pi^0\eta$ [34]. The yield of background events originating from $D_s^{*+}D_s^-$ ($B_{D_s^+}$) pairs is constrained to a Gaussian in the fit, with the mean and resolution fixed at (166 ± 9) . The mean of Gaussian is estimated from the inclusive MC sample, while the uncertainty is derived from the measured BFs of the main background processes $D_s^+ \rightarrow \pi^+\pi^0\eta$ [34] and $D_s^+ \rightarrow \pi^+\pi^0\pi^0$ [35]. The shape of the background components of non- $D_s^{*+}D_s^-$ reactions (B_{other}) is derived from the MC simulated events, and its yield is free in the fit.

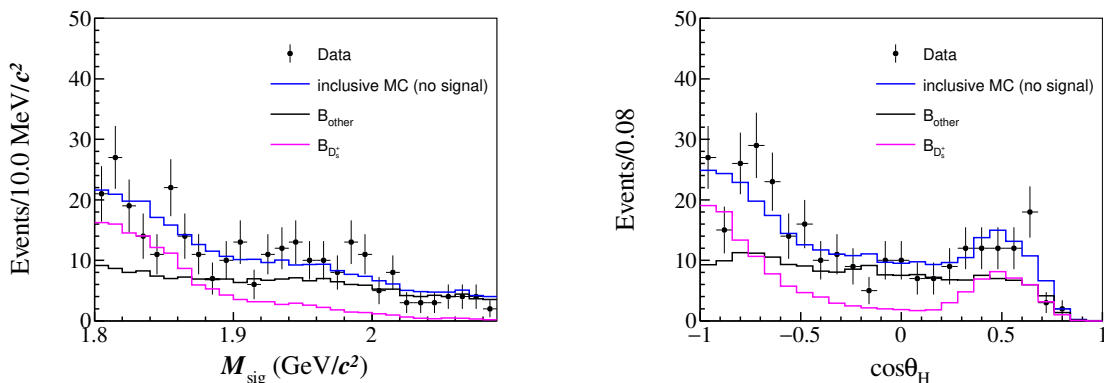


Figure 3. Distributions of $M_{D_s^+}$ and $\cos\theta_H$ of the DT candidate events for $D_s^+ \rightarrow \gamma\rho(770)^+$. The black points with error bars are data, the blue solid lines represent inclusive MC sample normalized to data, the magenta solid lines illustrate $B_{D_s^+}$, and the black solid lines illustrate B_{other} .

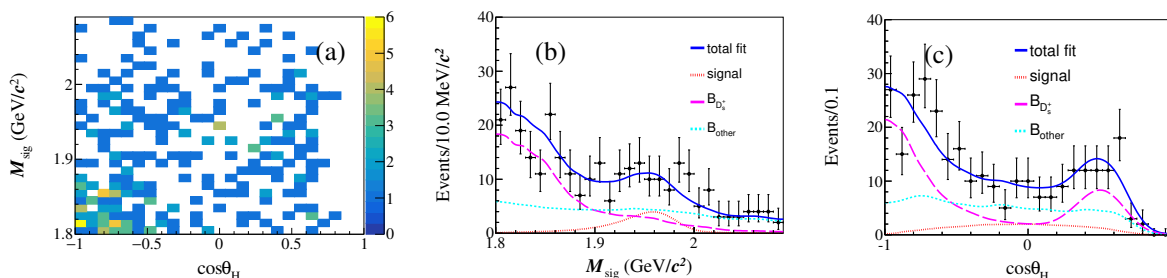


Figure 4. Distributions of M_{sig} versus $\cos\theta_H$ (a), M_{sig} (b) and $\cos\theta_H$ (c) for the DT candidate events of $D_s^+ \rightarrow \gamma\rho(770)^+$ at $E_{\text{cm}} = 4128 - 4226$ MeV. The black points with error bars are data, the blue solid curves are the total fit result, the red dotted lines are the signal contribution, the magenta long dashed lines illustrate $B_{D_s^+}$, and the cyan dashed lines illustrate B_{other} .

Tag mode	$\epsilon_I^{\text{DT}}(\%)$	$\epsilon_{\text{II}}^{\text{DT}}(\%)$	$\epsilon_{\text{III}}^{\text{DT}}(\%)$	$\epsilon_{\text{IV}}^{\text{DT}}(\%)$
$D_s^- \rightarrow K_S^0 K^-$	14.39 ± 0.28	14.68 ± 0.13	14.29 ± 0.16	14.66 ± 0.31
$D_s^- \rightarrow K^+ K^- \pi^-$	11.54 ± 0.11	11.79 ± 0.05	11.52 ± 0.06	11.72 ± 0.12
$D_s^- \rightarrow K^+ K^- \pi^- \pi^0$	3.38 ± 0.06	3.41 ± 0.02	3.42 ± 0.03	3.51 ± 0.06
$D_s^- \rightarrow K_S^0 K^+ \pi^- \pi^-$	5.77 ± 0.17	6.21 ± 0.08	6.24 ± 0.09	6.61 ± 0.20
$D_s^- \rightarrow K^- \pi^- \pi^+$	14.24 ± 0.37	13.38 ± 0.15	13.16 ± 0.18	13.82 ± 0.37

Table 5. The DT efficiencies ($\epsilon_{\alpha}^{\text{DT}}$) for the data samples taken at $E_{\text{cm}} = 4.128$ and 4.157 GeV (I), 4.178 GeV (II), from 4.189 to 4.219 GeV (III), and 4.226 GeV (IV).

From the 2D fit, the number of signal events is determined to be 33 ± 14 , with a statistical significance of 2.5σ . The statistical significance of the $D_s^+ \rightarrow \gamma\rho(770)^+$ decay is evaluated using $\sqrt{-2\ln(\mathcal{L}_0/\mathcal{L}_{\text{max}})}$, where \mathcal{L}_{max} is the maximum likelihood of the nominal fit and \mathcal{L}_0 is the likelihood of the fit without the signal component. The corresponding DT efficiencies for each tag mode are determined and listed in table 5. The BF of $D_s^+ \rightarrow \gamma\rho(770)^+$ is determined to be $(2.2 \pm 0.9) \times 10^{-4}$, where the uncertainty is statistical.

6 Systematic uncertainty

The systematic uncertainties in the BF measurement are discussed below. The additive systematic uncertainties only affect the fitted signal yield, while multiplicative systematic uncertainties affect the detection efficiency. Most systematic uncertainties related to the determination of the efficiency for reconstructing the ST side cancel out in the BF measurement due to the DT technique.

At first, the multiplicative systematic uncertainties are discussed below.

- **ST yield.** The total ST yield of all five ST modes is $495,398 \pm 1,900$, resulting in the statistical uncertainty of $\sqrt{1,900^2 - 495,398}/495,398 = 0.4\%$. Here, we only consider the statistical fluctuation related to the background of the ST side, as it is not correlated with the DT sample directly. Hence, a systematic uncertainty of 0.4% is assigned.
- **Tracking and PID.** The π^+ tracking and PID efficiencies are studied with $e^+e^- \rightarrow K^+K^-\pi^+\pi^-$ events. The systematic uncertainties are assigned as the data-MC differences of the π^+ PID and tracking efficiencies, which are both 1.0% [36].
- **γ reconstruction.** The uncertainty associated with the γ reconstruction efficiency is studied with the control sample of $J/\psi \rightarrow \pi^0\pi^+\pi^-$ [37]. The uncertainty due to the γ reconstruction is assigned as 1.0%.
- **π^0 reconstruction.** The systematic uncertainty associated with the π^0 reconstruction efficiency is investigated by using a control sample of the process $e^+e^- \rightarrow K^+K^-\pi^+\pi^-\pi^0$ [38]. The uncertainty due to the π^0 reconstruction is assigned as 2.0%.
- **MC statistics.** The uncertainty due to the limited signal MC sample size is obtained by $\sqrt{\sum_i (f_i \frac{\delta \epsilon_i}{\epsilon_i})^2}$, where f_i is the proportion of each ST yield to the total ST yield, and ϵ_i and $\delta \epsilon_i$ are the signal efficiency and the corresponding uncertainty of ST mode i , respectively. This uncertainty is found to be 0.4%.
- **$M_{\gamma\gamma_h}$ requirement and $M_{\gamma\gamma_{\text{extra}}}$ requirement.** The systematic uncertainties due to the $M_{\gamma\gamma_h}$ requirement and $M_{\gamma\gamma_{\text{extra}}}$ requirement are studied using a control sample of $D_s^+ \rightarrow \pi^+\pi^0\eta$ [34]. The differences in the efficiencies of the $M_{\gamma\gamma_h}$ requirement and $M_{\gamma\gamma_{\text{extra}}}$ requirement between data and MC simulation, 1.5% and 0.9%, are taken as the corresponding systematic uncertainties.
- **ρ^+ mass window.** The systematic uncertainties due to the ρ^+ mass window is studied using a control sample of $D^0 \rightarrow \pi^-\pi^0 e^+ \nu_e$ [39]. The differences in the efficiencies of the ρ^+ mass window between data and MC simulation, 1.0%, are taken as the corresponding systematic uncertainties.

The additive systematic uncertainties are discussed below.

- **Signal shape resolution.** To estimate the systematic uncertainty related with the signal shape resolution, we examine the BF by varying the mean and resolution of the convolving Gaussian function within their corresponding uncertainties. We take the

Category	Source	Uncertainty (%)
Multiplicative	ST yield	0.4
	Tracking	1.0
	PID	1.0
	π^0 and γ reconstructions	3.0
	MC statistics	0.4
	$M_{\gamma\gamma_h}$ requirement	1.5
	$M_{\gamma\gamma_{\text{extra}}}$ requirement	0.9
	$\rho(770)^+$ mass window	1.0
	Total	3.9
Additive	Signal shape resolution	6.4
	Background $B_{D_s^+}$	1.2
	Background B_{other}	7.2
	Total	9.7

Table 6. Systematic uncertainties in the BF measurement of $D_s^+ \rightarrow \gamma\rho(770)^+$.

change of the BF, 6.4%, as the systematic uncertainty. Among the results of these fits, the one corresponding to the largest upper limit on the branching fraction is chosen.

- **Background shape.** We vary the yield of the $B_{D_s^+}$ within corresponding uncertainty and assign the change of the BF of 1.2% as the systematic uncertainty. For B_{other} , we alter the MC-simulated shapes by varying the relative fractions of the two major background components from $q\bar{q}$ and non- $D_s^{*+}D_s^-$ open charm by $\pm 30\%$ [40], which is the statistical uncertainty of the individual cross section in data. The largest change of the BF, 7.2%, is taken as the systematic uncertainty. Among the variations, the fit resulting in the largest upper limit on the branching fraction is chosen.

The systematic uncertainties are summarised in table 6. Adding them in quadrature gives a total systematic uncertainty of the BF measurement of 10.5%.

The absolute BF of $D_s^+ \rightarrow \gamma\rho(770)^+$ is measured to be $(2.2 \pm 0.9 \pm 0.2) \times 10^{-4}$, where the first uncertainty is statistical and the second is systematic. Because of the limited statistics, an upper limit on the BF of $D_s^+ \rightarrow \gamma\rho(770)^+$ is also determined following ref. [19], after incorporating the systematic uncertainty via a likelihood scan method. To take into account the additive systematic uncertainties, the maximum-likelihood fits are repeated from the B_{other} shapes as mentioned in the previous section and the one resulting in the most conservative upper limit is chosen. Finally, the multiplicative systematic uncertainty σ_ϵ is incorporated in the calculation of the upper limit following refs. [41, 42].

$$L(\mathcal{B}) \propto \int_0^1 L(\mathcal{B} \cdot \frac{\epsilon}{\epsilon_0}) e^{-\frac{(\epsilon - \epsilon_0)^2}{2(\sigma_{\epsilon_0})^2}} d\epsilon, \tag{6.1}$$

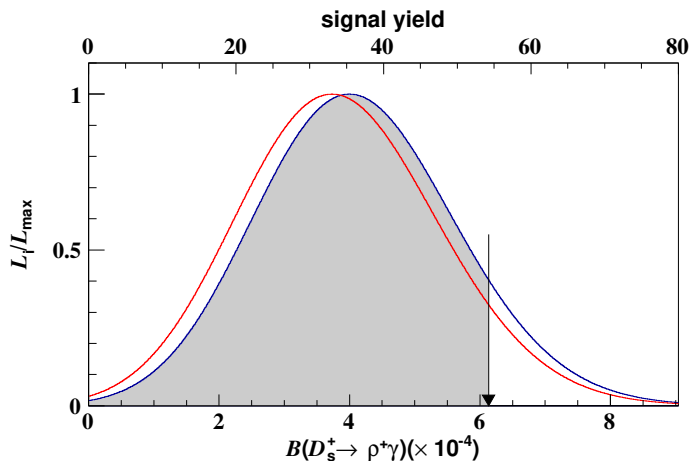


Figure 5. Normalized likelihood versus the signal yield and BF of $D_s^+ \rightarrow \gamma\rho(770)^+$. The red solid line is the likelihood curve for the nominal fit model, while the blue solid line represents the likelihood curve that gives the upper limit after incorporating the systematic uncertainty. The black arrow indicates the result corresponding to the 90% confidence level.

where $L(\mathcal{B})$ is the likelihood distribution as a function of assumed BFs; ϵ is the expected efficiency and ϵ_0 is the averaged MC-estimated efficiency. The likelihood distributions with and without incorporating the systematic uncertainties are shown in figure 5. The upper limit of the BF of $D_s^+ \rightarrow \gamma\rho(770)^+$ is obtained to be 6.1×10^{-4} at the 90% confidence level.

7 Summary

In summary, using 7.33 fb^{-1} of e^+e^- collision data collected with the BESIII detector between $E_{\text{cm}} = 4.128$ and 4.226 GeV , we search for the rare radiative decay $D_s^+ \rightarrow \gamma\rho(770)^+$ for the first time. A hint with a statistical significance of 2.5σ is obtained. The upper limit on the BF for $D_s^+ \rightarrow \gamma\rho(770)^+$ is estimated to be $\mathcal{B}(D_s^+ \rightarrow \gamma\rho(770)^+) < 6.1 \times 10^{-4}$ at the 90% confidence level, as shown in figure 5. The absolute BF of this decay is measured to be $\mathcal{B}(D_s^+ \rightarrow \gamma\rho(770)^+) = (2.2 \pm 0.9 \pm 0.2) \times 10^{-4}$, where the first uncertainty is statistical and the second is systematic. Figure 6 shows the comparison of our measurement with different theoretical predicted BFs. The obtained result in this analysis agrees with theoretical calculations based on light-cone sum rules [10], hybrid framework [4, 6] and vector-meson dominance [1]. However, it is 3.8σ smaller than the theoretical calculation of weak annihilation [13]. This study is beneficial for further understanding of the non-perturbative QCD in the D_s^+ sector.

Acknowledgments

The BESIII Collaboration thanks the staff of BEPCII and the IHEP computing center for their strong support. This work is supported in part by National Key R&D Program of China under Contracts Nos. 2020YFA0406400, 2020YFA0406300, 2023YFA1606000; National Natural Science Foundation of China (NSFC) under Contracts Nos. 12405094, 11635010, 11735014, 11935015, 11935016, 11935018, 12025502, 12035009, 12035013, 12061131003,

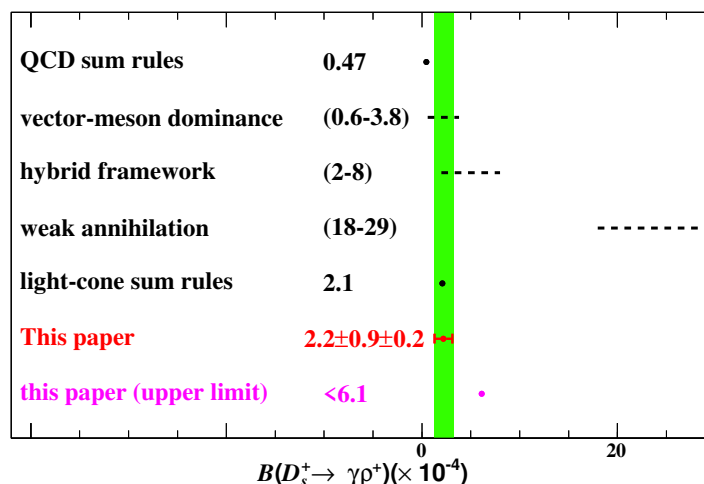


Figure 6. The comparison of $\mathcal{B}(D_s^+ \rightarrow \gamma\rho(770)^+)$ obtained in this work with theoretical calculations. The green band denotes the experimental result of this paper.

12192260, 12192261, 12192262, 12192263, 12192264, 12192265, 12221005, 12225509, 12235017, 12361141819; the Chinese Academy of Sciences (CAS) Large-Scale Scientific Facility Program; the CAS Center for Excellence in Particle Physics (CCEPP); Joint Large-Scale Scientific Facility Funds of the NSFC and CAS under Contract No. U1832207, U1932108, U2032104; 100 Talents Program of CAS; The Institute of Nuclear and Particle Physics (INPAC) and Shanghai Key Laboratory for Particle Physics and Cosmology; German Research Foundation DFG under Contracts Nos. 455635585, FOR5327, GRK 2149; Istituto Nazionale di Fisica Nucleare, Italy; Knut and Alice Wallenberg Foundation under Contracts Nos. 2021.0174, 2021.0299; Ministry of Development of Turkey under Contract No. DPT2006K-120470; National Research Foundation of Korea under Contract No. NRF-2022R1A2C1092335; National Science and Technology fund of Mongolia; National Science Research and Innovation Fund (NSRF) via the Program Management Unit for Human Resources & Institutional Development, Research and Innovation of Thailand under Contracts Nos. B16F640076, B50G670107; Polish National Science Centre under Contract No. 2019/35/O/ST2/02907; The Swedish Research Council; U.S. Department of Energy under Contract No. DE-FG02-05ER41374

Data Availability Statement. This article has no associated data or the data will not be deposited.

Code Availability Statement. This article has no associated code or the code will not be deposited.

Open Access. This article is distributed under the terms of the Creative Commons Attribution License ([CC-BY4.0](https://creativecommons.org/licenses/by/4.0/)), which permits any use, distribution and reproduction in any medium, provided the original author(s) and source are credited.

References

- [1] G. Burdman, E. Golowich, J.A.L. Hewett and S. Pakvasa, *Radiative weak decays of charm mesons*, *Phys. Rev. D* **52** (1995) 6383 [[hep-ph/9502329](#)] [[INSPIRE](#)].
- [2] CLEO collaboration, *Radiative decay modes of the D^0 meson*, *Phys. Rev. D* **58** (1998) 092001 [[hep-ex/9803022](#)] [[INSPIRE](#)].
- [3] B. Bajc, S. Fajfer and R.J. Oakes, *$C \rightarrow u\gamma$ in Cabibbo suppressed D meson radiative weak decays*, *Phys. Rev. D* **54** (1996) 5883 [[hep-ph/9509361](#)] [[INSPIRE](#)].
- [4] S. Fajfer and P. Singer, *Long distance $c \rightarrow u\gamma$ effects in weak radiative decays of D mesons*, *Phys. Rev. D* **56** (1997) 4302 [[hep-ph/9705327](#)] [[INSPIRE](#)].
- [5] W. Altmannshofer and F. Archilli, *Rare decays of b and c hadrons*, in the proceedings of the *Snowmass 2021*, Seattle, U.S.A., July 17–26 (2022) [[arXiv:2206.11331](#)] [[INSPIRE](#)].
- [6] S. Fajfer, S. Prelovsek and P. Singer, *Long distance contributions in $D \rightarrow V\gamma$ decays*, *Eur. Phys. J. C* **6** (1999) 471 [[hep-ph/9801279](#)] [[INSPIRE](#)].
- [7] BELLE collaboration, *Observation of radiative decay $D^0 \rightarrow \phi\gamma$* , *Phys. Rev. Lett.* **92** (2004) 101803 [[hep-ex/0308037](#)] [[INSPIRE](#)].
- [8] BELLE collaboration, *Observation of $D^0 \rightarrow \rho^0\gamma$ and search for CP violation in radiative charm decays*, *Phys. Rev. Lett.* **118** (2017) 051801 [[arXiv:1603.03257](#)] [[INSPIRE](#)].
- [9] BABAR collaboration, *Measurement of the Branching Fractions of the Radiative Charm Decays $D^0 \rightarrow \bar{K}^{*0}\gamma$ and $D^0 \rightarrow \phi\gamma$* , *Phys. Rev. D* **78** (2008) 071101 [[arXiv:0808.1838](#)] [[INSPIRE](#)].
- [10] J. Lyon and R. Zwicky, *$A_{CP}[D_{(s)}^{0,+} \rightarrow V\gamma]$ from Large \mathcal{O}_8* , *Phys. Rev. D* **106** (2022) 053001 [[arXiv:1210.6546](#)] [[INSPIRE](#)].
- [11] S. Fajfer, *Theoretical perspective on rare and radiative charm decays*, in the proceedings of the *7th International Workshop on Charm Physics*, Detroit, U.S.A., May 18–22 (2015) [[arXiv:1509.01997](#)] [[INSPIRE](#)].
- [12] A. Khodjamirian, G. Stoll and D. Wyler, *Calculation of long distance effects in exclusive weak radiative decays of B meson*, *Phys. Lett. B* **358** (1995) 129 [[hep-ph/9506242](#)] [[INSPIRE](#)].
- [13] S. de Boer and G. Hiller, *Rare radiative charm decays within the standard model and beyond*, *JHEP* **08** (2017) 091 [[arXiv:1701.06392](#)] [[INSPIRE](#)].
- [14] C. Yu et al., *BEPCII Performance and Beam Dynamics Studies on Luminosity*, in the proceedings of the *7th International Particle Accelerator Conference*, Busan, South Korea, May 08–13 (2016) [[DOI:10.18429/JACoW-IPAC2016-TUYA01](#)] [[INSPIRE](#)].
- [15] X. Li et al., *Study of MRPC technology for BESIII endcap-TOF upgrade*, *Radiat. Detect. Technol. Methods* **1** (2017) 13 [[INSPIRE](#)].
- [16] Y.-X. Guo et al., *The study of time calibration for upgraded end cap TOF of BESIII*, *Radiat. Detect. Technol. Methods* **1** (2017) 15 [[INSPIRE](#)].
- [17] P. Cao et al., *Design and construction of the new BESIII endcap Time-of-Flight system with MRPC Technology*, *Nucl. Instrum. Meth. A* **953** (2020) 163053 [[INSPIRE](#)].
- [18] CLEO collaboration, *Measurement of Charm Production Cross Sections in e^+e^- Annihilation at Energies between 3.97 and 4.26-GeV*, *Phys. Rev. D* **80** (2009) 072001 [[arXiv:0801.3418](#)] [[INSPIRE](#)].
- [19] BESIII collaboration, *Search for the semileptonic decay $D_s^+ \rightarrow \pi^0 e^+ \nu_e$* , *Phys. Rev. D* **106** (2022) 112004 [[arXiv:2206.13870](#)] [[INSPIRE](#)].

- [20] BESIII collaboration, *Measurements of the center-of-mass energies of collisions at BESIII*, *Chin. Phys. C* **45** (2021) 103001 [[arXiv:2012.14750](#)] [[INSPIRE](#)].
- [21] BESIII collaboration, *Measurement of the center-of-mass energies at BESIII via the di-muon process*, *Chin. Phys. C* **40** (2016) 063001 [[arXiv:1510.08654](#)] [[INSPIRE](#)].
- [22] BESIII collaboration, *Measurement of integrated luminosities at BESIII for data samples at center-of-mass energies between 4.0 and 4.6 GeV*, *Chin. Phys. C* **46** (2022) 113002 [[arXiv:2203.03133](#)] [[INSPIRE](#)].
- [23] GEANT4 collaboration, *GEANT4 — a simulation toolkit*, *Nucl. Instrum. Meth. A* **506** (2003) 250 [[INSPIRE](#)].
- [24] S. Jadach, B.F.L. Ward and Z. Was, *Coherent exclusive exponentiation for precision Monte Carlo calculations*, *Phys. Rev. D* **63** (2001) 113009 [[hep-ph/0006359](#)] [[INSPIRE](#)].
- [25] S. Jadach, B.F.L. Ward and Z. Was, *The Precision Monte Carlo event generator KK for two fermion final states in e^+e^- collisions*, *Comput. Phys. Commun.* **130** (2000) 260 [[hep-ph/9912214](#)] [[INSPIRE](#)].
- [26] D.J. Lange, *The EvtGen particle decay simulation package*, *Nucl. Instrum. Meth. A* **462** (2001) 152 [[INSPIRE](#)].
- [27] R.-G. Ping, *Event generators at BESIII*, *Chin. Phys. C* **32** (2008) 599 [[INSPIRE](#)].
- [28] PARTICLE DATA GROUP collaboration, *Review of Particle Physics (2023)*, <https://pdg.lbl.gov/index-2023.html>.
- [29] J.C. Chen et al., *Event generator for J/ψ and $\psi(2S)$ decay*, *Phys. Rev. D* **62** (2000) 034003 [[INSPIRE](#)].
- [30] R.-L. Yang, R.-G. Ping and H. Chen, *Tuning and Validation of the Lundcharm Model with J/ψ Decays*, *Chin. Phys. Lett.* **31** (2014) 061301 [[INSPIRE](#)].
- [31] E. Richter-Was, *QED bremsstrahlung in semileptonic B and leptonic tau decays*, *Phys. Lett. B* **303** (1993) 163 [[INSPIRE](#)].
- [32] MARK-III collaboration, *Direct Measurements of Charmed d Meson Hadronic Branching Fractions*, *Phys. Rev. Lett.* **56** (1986) 2140 [[INSPIRE](#)].
- [33] G. Punzi, *Sensitivity optimization of multichannel searches for new signals*, [arXiv:2011.11770](#) [[INSPIRE](#)].
- [34] BESIII collaboration, *Amplitude analysis of $D_s^+ \rightarrow \pi^+\pi^0\eta$ and first observation of the pure W-annihilation decays $D_s^+ \rightarrow a_0(980)^+\pi^0$ and $D_s^+ \rightarrow a_0(980)^0\pi^+$* , *Phys. Rev. Lett.* **123** (2019) 112001 [[arXiv:1903.04118](#)] [[INSPIRE](#)].
- [35] BESIII collaboration, *Amplitude analysis and branching fraction measurement of the decay $D_s^+ \rightarrow \pi^+\pi^0\pi^0$* , *JHEP* **01** (2022) 052 [[arXiv:2109.12660](#)] [[INSPIRE](#)].
- [36] BESIII collaboration, *Amplitude analysis and branching fraction measurement of $D_s^+ \rightarrow K^+K^-\pi^+$* , *Phys. Rev. D* **104** (2021) 012016 [[arXiv:2011.08041](#)] [[INSPIRE](#)].
- [37] BESIII collaboration, *Study of χ_{cJ} radiative decays into a vector meson*, *Phys. Rev. D* **83** (2011) 112005 [[arXiv:1103.5564](#)] [[INSPIRE](#)].
- [38] BESIII collaboration, *Observation of the decay $D_s^+ \rightarrow \omega\pi^+\eta$* , *Phys. Rev. D* **107** (2023) 052010 [[arXiv:2302.04670](#)] [[INSPIRE](#)].
- [39] BESIII collaboration, *Observation of $D^+ \rightarrow f_0(500)e^+\nu_e$ and Improved Measurements of $D \rightarrow \rho e^+\nu_e$* , *Phys. Rev. Lett.* **122** (2019) 062001 [[arXiv:1809.06496](#)] [[INSPIRE](#)].

- [40] BESIII collaboration, *Amplitude analysis and branching-fraction measurement of $D_s^+ \rightarrow K_S^0 \pi^+ \pi^0$* , *JHEP* **06** (2021) 181 [[arXiv:2103.15098](#)] [[INSPIRE](#)].
- [41] K. Stenson, *A more exact solution for incorporating multiplicative systematic uncertainties in branching ratio limits*, [physics/0605236](#) [[INSPIRE](#)].
- [42] X.-X. Liu, X.-R. Lü and Y.-S. Zhu, *Combined estimation for multi-measurements of branching ratio*, *Chin. Phys. C* **39** (2015) 103001 [[arXiv:1505.01278](#)] [[INSPIRE](#)].

The BESIII collaboration

M. Ablikim¹, M.N. Achasov^{4,c}, P. Adlarson⁷⁶, O. Afedulidis³, X.C. Ai⁸¹, R. Aliberti³⁵,
A. Amoroso^{75A,75C}, Q. An^{72,58,a}, Y. Bai⁵⁷, O. Bakina³⁶, I. Balossino^{29A}, Y. Ban^{46,h}, H.-R. Bao⁶⁴,
V. Batozskaya^{1,44}, K. Begzsuren³², N. Berger³⁵, M. Berlowski⁴⁴, M. Bertani^{28A}, D. Bettoni^{29A},
F. Bianchi^{75A,75C}, E. Bianco^{75A,75C}, A. Bortone^{75A,75C}, I. Boyko³⁶, R.A. Briere⁵, A. Brueggemann⁶⁹,
H. Cai⁷⁷, X. Cai^{1,58}, A. Calcaterra^{28A}, G.F. Cao^{1,64}, N. Cao^{1,64}, S.A. Cetin^{62A}, X.Y. Chai^{46,h},
J.F. Chang^{1,58}, G.R. Che⁴³, Y.Z. Che^{1,58,64}, G. Chelkov^{36,b}, C. Chen⁴³, C.H. Chen⁹, Chao Chen⁵⁵,
G. Chen¹, H.S. Chen^{1,64}, H.Y. Chen²⁰, M.L. Chen^{1,58,64}, S.J. Chen⁴², S.L. Chen⁴⁵, S.M. Chen⁶¹,
T. Chen^{1,64}, X.R. Chen^{31,64}, X.T. Chen^{1,64}, Y.B. Chen^{1,58}, Y.Q. Chen³⁴, Z.J. Chen^{25,i},
Z.Y. Chen^{1,64}, S.K. Choi¹⁰, G. Cibinetto^{29A}, F. Cossio^{75C}, J.J. Cui⁵⁰, H.L. Dai^{1,58}, J.P. Dai⁷⁹,
A. Dbeyssi¹⁸, R. E. de Boer³, D. Dedovich³⁶, C.Q. Deng⁷³, Z.Y. Deng¹, A. Denig³⁵, I. Denysenko³⁶,
M. Destefanis^{75A,75C}, F. De Mori^{75A,75C}, B. Ding^{67,1}, X.X. Ding^{46,h}, Y. Ding³⁴, Y. Ding⁴⁰,
J. Dong^{1,58}, L.Y. Dong^{1,64}, M.Y. Dong^{1,58,64}, X. Dong⁷⁷, M.C. Du¹, S.X. Du⁸¹, Y.Y. Duan⁵⁵,
Z.H. Duan⁴², P. Egorov^{36,b}, Y.H. Fan⁴⁵, J. Fang^{1,58}, J. Fang⁵⁹, S.S. Fang^{1,64}, W.X. Fang¹, Y. Fang¹,
Y.Q. Fang^{1,58}, R. Farinelli^{29A}, L. Fava^{75B,75C}, F. Feldbauer³, G. Felici^{28A}, C.Q. Feng^{72,58},
J.H. Feng⁵⁹, Y.T. Feng^{72,58}, M. Fritsch³, C.D. Fu¹, J.L. Fu⁶⁴, Y.W. Fu^{1,64}, H. Gao⁶⁴, X.B. Gao⁴¹,
Y.N. Gao^{46,h}, Yang Gao^{72,58}, S. Garbolino^{75C}, I. Garzia^{29A,29B}, L. Ge⁸¹, P.T. Ge¹⁹, Z.W. Ge⁴²,
C. Geng⁵⁹, E.M. Gersabeck⁶⁸, A. Gilman⁷⁰, K. Goetzen¹³, L. Gong⁴⁰, W.X. Gong^{1,58}, W. Gradl³⁵,
S. Gramigna^{29A,29B}, M. Greco^{75A,75C}, M.H. Gu^{1,58}, Y.T. Gu¹⁵, C.Y. Guan^{1,64}, A.Q. Guo^{31,64},
L.B. Guo⁴¹, M.J. Guo⁵⁰, R.P. Guo⁴⁹, Y.P. Guo^{12,g}, A. Guskov^{36,b}, J. Gutierrez²⁷, K.L. Han⁶⁴,
T.T. Han¹, F. Hanisch³, X.Q. Hao¹⁹, F.A. Harris⁶⁶, K.K. He⁵⁵, K.L. He^{1,64}, F.H. Heinsius³,
C.H. Heinz³⁵, Y.K. Heng^{1,58,64}, C. Herold⁶⁰, T. Holtmann³, P.C. Hong³⁴, G.Y. Hou^{1,64}, X.T. Hou^{1,64},
Y.R. Hou⁶⁴, Z.L. Hou¹, B.Y. Hu⁵⁹, H.M. Hu^{1,64}, J.F. Hu^{56,j}, S.L. Hu^{12,g}, T. Hu^{1,58,64}, Y. Hu¹,
G.S. Huang^{72,58}, K.X. Huang⁵⁹, L.Q. Huang^{31,64}, X.T. Huang⁵⁰, Y.P. Huang¹, Y.S. Huang⁵⁹,
T. Hussain⁷⁴, F. Hölzken³, N. Hüsken³⁵, N. in der Wiesche⁶⁹, J. Jackson²⁷, S. Janchiv³², J.H. Jeong¹⁰,
Q. Ji¹, Q.P. Ji¹⁹, W. Ji^{1,64}, X.B. Ji^{1,64}, X.L. Ji^{1,58}, Y.Y. Ji⁵⁰, X.Q. Jia⁵⁰, Z.K. Jia^{72,58}, D. Jiang^{1,64},
H.B. Jiang⁷⁷, P.C. Jiang^{46,h}, S.S. Jiang³⁹, T.J. Jiang¹⁶, X.S. Jiang^{1,58,64}, Y. Jiang⁶⁴, J.B. Jiao⁵⁰,
J.K. Jiao³⁴, Z. Jiao²³, S. Jin⁴², Y. Jin⁶⁷, M.Q. Jing^{1,64}, X.M. Jing⁶⁴, T. Johansson⁷⁶, S. Kabana³³,
N. Kalantar-Nayestanaki⁶⁵, X.L. Kang⁹, X.S. Kang⁴⁰, M. Kavatsyuk⁶⁵, B.C. Ke⁸¹, V. Khachatryan²⁷,
A. Khoukaz⁶⁹, R. Kiuchi¹, O.B. Kolcu^{62A}, B. Kopf³, M. Kuessner³, X. Kui^{1,64}, N. Kumar²⁶,
A. Kupsc^{44,76}, W. Kühn³⁷, J.J. Lane⁶⁸, L. Lavezzi^{75A,75C}, T.T. Lei^{72,58}, Z.H. Lei^{72,58}, M. Lellmann³⁵,
T. Lenz³⁵, C. Li⁴³, C. Li⁴⁷, C.H. Li³⁹, Cheng Li^{72,58}, D.M. Li⁸¹, F. Li^{1,58}, G. Li¹, H.B. Li^{1,64},
H.J. Li¹⁹, H.N. Li^{56,j}, Hui Li⁴³, J.R. Li⁶¹, J.S. Li⁵⁹, K. Li¹, K.L. Li¹⁹, L.J. Li^{1,64}, L.K. Li¹, Lei Li⁴⁸,
M.H. Li⁴³, P.R. Li^{38,k,l}, Q.M. Li^{1,64}, Q.X. Li⁵⁰, R. Li^{17,31}, S.X. Li¹², T. Li⁵⁰, W.D. Li^{1,64}, W.G. Li^{1,a},
X. Li^{1,64}, X.H. Li^{72,58}, X.L. Li⁵⁰, X.Y. Li^{1,64}, X.Z. Li⁵⁹, Y.G. Li^{46,h}, Z.J. Li⁵⁹, Z.Y. Li⁷⁹, C. Liang⁴²,
H. Liang^{72,58}, H. Liang^{1,64}, Y.F. Liang⁵⁴, Y.T. Liang^{31,64}, G.R. Liao¹⁴, Y.P. Liao^{1,64}, J. Libby²⁶, A.
Limphirat⁶⁰, C.C. Lin⁵⁵, D.X. Lin^{31,64}, T. Lin¹, B.J. Liu¹, B.X. Liu⁷⁷, C. Liu³⁴, C.X. Liu¹, F. Liu¹,
F.H. Liu⁵³, Feng Liu⁶, G.M. Liu^{56,j}, H. Liu^{38,k,l}, H.B. Liu¹⁵, H.H. Liu¹, H.M. Liu^{1,64}, Huihui Liu²¹,
J.B. Liu^{72,58}, J.Y. Liu^{1,64}, K. Liu^{38,k,l}, K.Y. Liu⁴⁰, Ke Liu²², L. Liu^{72,58}, L.C. Liu⁴³, Lu Liu⁴³,
M.H. Liu^{12,g}, P.L. Liu¹, Q. Liu⁶⁴, S.B. Liu^{72,58}, T. Liu^{12,g}, W.K. Liu⁴³, W.M. Liu^{72,58}, X. Liu³⁹,
X. Liu^{38,k,l}, Y. Liu⁸¹, Y. Liu^{38,k,l}, Y.B. Liu⁴³, Z.A. Liu^{1,58,64}, Z.D. Liu⁹, Z.Q. Liu⁵⁰, X.C. Lou^{1,58,64},
F.X. Lu⁵⁹, H.J. Lu²³, J.G. Lu^{1,58}, X.L. Lu¹, Y. Lu⁷, Y.P. Lu^{1,58}, Z.H. Lu^{1,64}, C.L. Luo⁴¹, J.R. Luo⁵⁹,

M.X. Luo⁸⁰, T. Luo^{12,g}, X.L. Luo^{1,58}, X.R. Lyu⁶⁴, Y.F. Lyu⁴³, F.C. Ma⁴⁰, H. Ma⁷⁹, H.L. Ma¹,
 J.L. Ma^{1,64}, L.L. Ma⁵⁰, L.R. Ma⁶⁷, M.M. Ma^{1,64}, Q.M. Ma¹, R.Q. Ma^{1,64}, T. Ma^{72,58}, X.T. Ma^{1,64},
 X.Y. Ma^{1,58}, Y.M. Ma³¹, F.E. Maas¹⁸, I. MacKay⁷⁰, M. Maggiora^{75A,75C}, S. Malde⁷⁰, Y.J. Mao^{46,h},
 Z.P. Mao¹, S. Marcello^{75A,75C}, Z.X. Meng⁶⁷, J.G. Messendorp^{13,65}, G. Mezzadri^{29A}, H. Miao^{1,64},
 T.J. Min⁴², R.E. Mitchell²⁷, X.H. Mo^{1,58,64}, B. Moses²⁷, N. Yu. Muchnoi^{4,c}, J. Muskalla³⁵,
 Y. Nefedov³⁶, F. Nerling^{18,e}, L.S. Nie²⁰, I.B. Nikolaev^{4,c}, Z. Ning^{1,58}, S. Nisar^{11,m}, Q.L. Niu^{38,k,l},
 W.D. Niu⁵⁵, Y. Niu⁵⁰, S.L. Olsen⁶⁴, S.L. Olsen^{10,64}, Q. Ouyang^{1,58,64}, S. Pacetti^{28B,28C}, X. Pan⁵⁵,
 Y. Pan⁵⁷, A. Pathak³⁴, Y.P. Pei^{72,58}, M. Pelizaesus³, H.P. Peng^{72,58}, Y.Y. Peng^{38,k,l}, K. Peters^{13,e},
 J.L. Ping⁴¹, R.G. Ping^{1,64}, S. Plura³⁵, V. Prasad³³, F.Z. Qi¹, H. Qi^{72,58}, H.R. Qi⁶¹, M. Qi⁴²,
 T.Y. Qi^{12,g}, S. Qian^{1,58}, W.B. Qian⁶⁴, C.F. Qiao⁶⁴, X.K. Qiao⁸¹, J.J. Qin⁷³, L.Q. Qin¹⁴,
 L.Y. Qin^{72,58}, X.P. Qin^{12,g}, X.S. Qin⁵⁰, Z.H. Qin^{1,58}, J.F. Qiu¹, Z.H. Qu⁷³, C.F. Redmer³⁵,
 K.J. Ren³⁹, A. Rivetti^{75C}, M. Rolo^{75C}, G. Rong^{1,64}, Ch. Rosner¹⁸, M.Q. Ruan^{1,58}, S.N. Ruan⁴³,
 N. Salone⁴⁴, A. Sarantsev^{36,d}, Y. Schelhaas³⁵, K. Schoenning⁷⁶, M. Scodreggio^{29A}, K.Y. Shan^{12,g},
 W. Shan²⁴, X.Y. Shan^{72,58}, Z.J. Shang^{38,k,l}, J.F. Shangguan¹⁶, L.G. Shao^{1,64}, M. Shao^{72,58},
 C.P. Shen^{12,g}, H.F. Shen^{1,8}, W.H. Shen⁶⁴, X.Y. Shen^{1,64}, B.A. Shi⁶⁴, H. Shi^{72,58}, H.C. Shi^{72,58},
 J.L. Shi^{12,g}, J.Y. Shi¹, Q.Q. Shi⁵⁵, S.Y. Shi⁷³, X. Shi^{1,58}, J.J. Song¹⁹, T.Z. Song⁵⁹, W.M. Song^{34,1}, Y.
 J. Song^{12,g}, Y.X. Song^{46,h,n}, S. Sosio^{75A,75C}, S. Spataro^{75A,75C}, F. Stieler³⁵, S. S. Su⁴⁰, Y.J. Su⁶⁴,
 G.B. Sun⁷⁷, G.X. Sun¹, H. Sun⁶⁴, H.K. Sun¹, J.F. Sun¹⁹, K. Sun⁶¹, L. Sun⁷⁷, S.S. Sun^{1,64}, T. Sun^{51,f},
 W.Y. Sun³⁴, Y. Sun⁹, Y.J. Sun^{72,58}, Y.Z. Sun¹, Z.Q. Sun^{1,64}, Z.T. Sun⁵⁰, C.J. Tang⁵⁴, G.Y. Tang¹,
 J. Tang⁵⁹, M. Tang^{72,58}, Y.A. Tang⁷⁷, L.Y. Tao⁷³, Q.T. Tao^{25,i}, M. Tat⁷⁰, J.X. Teng^{72,58},
 V. Thoren⁷⁶, W.H. Tian⁵⁹, Y. Tian^{31,64}, Z.F. Tian⁷⁷, I. Uman^{62B}, Y. Wan⁵⁵, S.J. Wang⁵⁰, B. Wang¹,
 B.L. Wang⁶⁴, Bo Wang^{72,58}, D.Y. Wang^{46,h}, F. Wang⁷³, H.J. Wang^{38,k,l}, J.J. Wang⁷⁷, J.P. Wang⁵⁰,
 K. Wang^{1,58}, L.L. Wang¹, M. Wang⁵⁰, N.Y. Wang⁶⁴, S. Wang^{38,k,l}, S. Wang^{12,g}, T. Wang^{12,g},
 T.J. Wang⁴³, W. Wang⁵⁹, W. Wang⁷³, W.P. Wang^{35,58,72,o}, X. Wang^{46,h}, X.F. Wang^{38,k,l},
 X.J. Wang³⁹, X.L. Wang^{12,g}, X.N. Wang¹, Y. Wang⁶¹, Y.D. Wang⁴⁵, Y.F. Wang^{1,58,64}, Y.L. Wang¹⁹,
 Y.N. Wang⁴⁵, Y.Q. Wang¹, Yaqian Wang¹⁷, Yi Wang⁶¹, Z. Wang^{1,58}, Z.L. Wang⁷³, Z.Y. Wang^{1,64},
 Ziyi Wang⁶⁴, D.H. Wei¹⁴, F. Weidner⁶⁹, S.P. Wen¹, Y.R. Wen³⁹, U. Wiedner³, G. Wilkinson⁷⁰,
 M. Wolke⁷⁶, L. Wollenberg³, C. Wu³⁹, J.F. Wu^{1,8}, L.H. Wu¹, L.J. Wu^{1,64}, X. Wu^{12,g}, X.H. Wu³⁴,
 Y. Wu^{72,58}, Y.H. Wu⁵⁵, Y.J. Wu³¹, Z. Wu^{1,58}, L. Xia^{72,58}, X.M. Xian³⁹, B.H. Xiang^{1,64}, T. Xiang^{46,h},
 D. Xiao^{38,k,l}, G.Y. Xiao⁴², S.Y. Xiao¹, Y. L. Xiao^{12,g}, Z.J. Xiao⁴¹, C. Xie⁴², X.H. Xie^{46,h}, Y. Xie⁵⁰,
 Y.G. Xie^{1,58}, Y.H. Xie⁶, Z.P. Xie^{72,58}, T.Y. Xing^{1,64}, C.F. Xu^{1,64}, C.J. Xu⁵⁹, G.F. Xu¹, H.Y. Xu^{67,2,p},
 M. Xu^{72,58}, Q.J. Xu¹⁶, Q.N. Xu³⁰, W. Xu¹, W.L. Xu⁶⁷, X.P. Xu⁵⁵, Y. Xu⁴⁰, Y.C. Xu⁷⁸, Z.S. Xu⁶⁴,
 F. Yan^{12,g}, L. Yan^{12,g}, W.B. Yan^{72,58}, W.C. Yan⁸¹, X.Q. Yan^{1,64}, H.J. Yang^{51,f}, H.L. Yang³⁴,
 H.X. Yang¹, J.H. Yang⁴², T. Yang¹, Y. Yang^{12,g}, Y.F. Yang⁴³, Y.F. Yang^{1,64}, Y.X. Yang^{1,64},
 Z.W. Yang^{38,k,l}, Z.P. Yao⁵⁰, M. Ye^{1,58}, M.H. Ye⁸, J.H. Yin¹, Junhao Yin⁴³, Z.Y. You⁵⁹,
 B.X. Yu^{1,58,64}, C.X. Yu⁴³, G. Yu^{1,64}, J.S. Yu^{25,i}, M.C. Yu⁴⁰, T. Yu⁷³, X.D. Yu^{46,h}, Y.C. Yu⁸¹,
 C.Z. Yuan^{1,64}, J. Yuan³⁴, J. Yuan⁴⁵, L. Yuan², S.C. Yuan^{1,64}, Y. Yuan^{1,64}, Z.Y. Yuan⁵⁹, C.X. Yue³⁹,
 A.A. Zafar⁷⁴, F.R. Zeng⁵⁰, S.H. Zeng^{63A,63B,63C,63D}, X. Zeng^{12,g}, Y. Zeng^{25,i}, Y.J. Zeng⁵⁹,
 Y.J. Zeng^{1,64}, X.Y. Zhai³⁴, Y.C. Zhai⁵⁰, Y.H. Zhan⁵⁹, A.Q. Zhang^{1,64}, B.L. Zhang^{1,64}, B.X. Zhang¹,
 D.H. Zhang⁴³, G.Y. Zhang¹⁹, H. Zhang⁸¹, H. Zhang^{72,58}, H.C. Zhang^{1,58,64}, H.H. Zhang⁵⁹,
 H.H. Zhang³⁴, H.Q. Zhang^{1,58,64}, H.R. Zhang^{72,58}, H.Y. Zhang^{1,58}, J. Zhang⁸¹, J. Zhang⁵⁹,
 J.J. Zhang⁵², J.L. Zhang²⁰, J.Q. Zhang⁴¹, J.S. Zhang^{12,g}, J.W. Zhang^{1,58,64}, J.X. Zhang^{38,k,l},
 J.Y. Zhang¹, J.Z. Zhang^{1,64}, Jianyu Zhang⁶⁴, L.M. Zhang⁶¹, Lei Zhang⁴², N Zhang⁸¹, P. Zhang^{1,64},

Q.Y. Zhang³⁴, R.Y. Zhang^{38,k,l}, S.H. Zhang^{1,64}, Shulei Zhang^{25,i}, X.M. Zhang¹, X. Y Zhang⁴⁰, X.Y. Zhang⁵⁰, Y. Zhang¹, Y. Zhang⁷³, Y. T. Zhang⁸¹, Y.H. Zhang^{1,58}, Y.M. Zhang³⁹, Yan Zhang^{72,58}, Z.D. Zhang¹, Z.H. Zhang¹, Z.L. Zhang³⁴, Z.Y. Zhang⁷⁷, Z.Y. Zhang⁴³, Z.Z. Zhang⁴⁵, G. Zhao¹, J.Y. Zhao^{1,64}, J.Z. Zhao^{1,58}, L. Zhao¹, Lei Zhao^{72,58}, M.G. Zhao⁴³, N. Zhao⁷⁹, R.P. Zhao⁶⁴, S.J. Zhao⁸¹, Y.B. Zhao^{1,58}, Y.X. Zhao^{31,64}, Z.G. Zhao^{72,58}, A. Zhemchugov^{36,b}, B. Zheng⁷³, B.M. Zheng³⁴, J.P. Zheng^{1,58}, W.J. Zheng^{1,64}, Y.H. Zheng⁶⁴, B. Zhong⁴¹, X. Zhong⁵⁹, H. Zhou⁵⁰, J.Y. Zhou³⁴, L.P. Zhou^{1,64}, S. Zhou⁶, X. Zhou⁷⁷, X.K. Zhou⁶, X.R. Zhou^{72,58}, X.Y. Zhou³⁹, Y.Z. Zhou^{12,g}, Z.C. Zhou²⁰, A.N. Zhu⁶⁴, J. Zhu⁴³, K. Zhu¹, K.J. Zhu^{1,58,64}, K.S. Zhu^{12,g}, L. Zhu³⁴, L.X. Zhu⁶⁴, S.H. Zhu⁷¹, T.J. Zhu^{12,g}, W.D. Zhu⁴¹, Y.C. Zhu^{72,58}, Z.A. Zhu^{1,64}, J.H. Zou¹, J. Zu^{72,58}

¹ *Institute of High Energy Physics, Beijing 100049, People's Republic of China*

² *Beihang University, Beijing 100191, People's Republic of China*

³ *Bochum Ruhr-University, D-44780 Bochum, Germany*

⁴ *Budker Institute of Nuclear Physics SB RAS (BINP), Novosibirsk 630090, Russia*

⁵ *Carnegie Mellon University, Pittsburgh, Pennsylvania 15213, U.S.A.*

⁶ *Central China Normal University, Wuhan 430079, People's Republic of China*

⁷ *Central South University, Changsha 410083, People's Republic of China*

⁸ *China Center of Advanced Science and Technology, Beijing 100190, People's Republic of China*

⁹ *China University of Geosciences, Wuhan 430074, People's Republic of China*

¹⁰ *Chung-Ang University, Seoul, 06974, Republic of Korea*

¹¹ *COMSATS University Islamabad, Lahore Campus, Defence Road, Off Raiwind Road, 54000 Lahore, Pakistan*

¹² *Fudan University, Shanghai 200433, People's Republic of China*

¹³ *GSI Helmholtzcentre for Heavy Ion Research GmbH, D-64291 Darmstadt, Germany*

¹⁴ *Guangxi Normal University, Guilin 541004, People's Republic of China*

¹⁵ *Guangxi University, Nanning 530004, People's Republic of China*

¹⁶ *Hangzhou Normal University, Hangzhou 310036, People's Republic of China*

¹⁷ *Hebei University, Baoding 071002, People's Republic of China*

¹⁸ *Helmholtz Institute Mainz, Staudinger Weg 18, D-55099 Mainz, Germany*

¹⁹ *Henan Normal University, Xinxiang 453007, People's Republic of China*

²⁰ *Henan University, Kaifeng 475004, People's Republic of China*

²¹ *Henan University of Science and Technology, Luoyang 471003, People's Republic of China*

²² *Henan University of Technology, Zhengzhou 450001, People's Republic of China*

²³ *Huangshan College, Huangshan 245000, People's Republic of China*

²⁴ *Hunan Normal University, Changsha 410081, People's Republic of China*

²⁵ *Hunan University, Changsha 410082, People's Republic of China*

²⁶ *Indian Institute of Technology Madras, Chennai 600036, India*

²⁷ *Indiana University, Bloomington, Indiana 47405, U.S.A.*

²⁸ *INFN Laboratori Nazionali di Frascati, (A)INFN Laboratori Nazionali di Frascati, I-00044, Frascati, Italy; (B)INFN Sezione di Perugia, I-06100, Perugia, Italy; (C)University of Perugia, I-06100, Perugia, Italy*

²⁹ *INFN Sezione di Ferrara, (A)INFN Sezione di Ferrara, I-44122, Ferrara, Italy; (B)University of Ferrara, I-44122, Ferrara, Italy*

³⁰ *Inner Mongolia University, Hohhot 010021, People's Republic of China*

³¹ *Institute of Modern Physics, Lanzhou 730000, People's Republic of China*

³² *Institute of Physics and Technology, Peace Avenue 54B, Ulaanbaatar 13330, Mongolia*

³³ *Instituto de Alta Investigación, Universidad de Tarapacá, Casilla 7D, Arica 1000000, Chile*

³⁴ *Jilin University, Changchun 130012, People's Republic of China*

³⁵ *Johannes Gutenberg University of Mainz, Johann-Joachim-Becher-Weg 45, D-55099 Mainz, Germany*

³⁶ *Joint Institute for Nuclear Research, 141980 Dubna, Moscow region, Russia*

³⁷ *Justus-Liebig-Universität Giessen, II. Physikalisches Institut, Heinrich-Buff-Ring 16, D-35392 Giessen, Germany*

- ³⁸ Lanzhou University, Lanzhou 730000, People's Republic of China
- ³⁹ Liaoning Normal University, Dalian 116029, People's Republic of China
- ⁴⁰ Liaoning University, Shenyang 110036, People's Republic of China
- ⁴¹ Nanjing Normal University, Nanjing 210023, People's Republic of China
- ⁴² Nanjing University, Nanjing 210093, People's Republic of China
- ⁴³ Nankai University, Tianjin 300071, People's Republic of China
- ⁴⁴ National Centre for Nuclear Research, Warsaw 02-093, Poland
- ⁴⁵ North China Electric Power University, Beijing 102206, People's Republic of China
- ⁴⁶ Peking University, Beijing 100871, People's Republic of China
- ⁴⁷ Qufu Normal University, Qufu 273165, People's Republic of China
- ⁴⁸ Renmin University of China, Beijing 100872, People's Republic of China
- ⁴⁹ Shandong Normal University, Jinan 250014, People's Republic of China
- ⁵⁰ Shandong University, Jinan 250100, People's Republic of China
- ⁵¹ Shanghai Jiao Tong University, Shanghai 200240, People's Republic of China
- ⁵² Shanxi Normal University, Linfen 041004, People's Republic of China
- ⁵³ Shanxi University, Taiyuan 030006, People's Republic of China
- ⁵⁴ Sichuan University, Chengdu 610064, People's Republic of China
- ⁵⁵ Soochow University, Suzhou 215006, People's Republic of China
- ⁵⁶ South China Normal University, Guangzhou 510006, People's Republic of China
- ⁵⁷ Southeast University, Nanjing 211100, People's Republic of China
- ⁵⁸ State Key Laboratory of Particle Detection and Electronics, Beijing 100049, Hefei 230026, People's Republic of China
- ⁵⁹ Sun Yat-Sen University, Guangzhou 510275, People's Republic of China
- ⁶⁰ Suranaree University of Technology, University Avenue 111, Nakhon Ratchasima 30000, Thailand
- ⁶¹ Tsinghua University, Beijing 100084, People's Republic of China
- ⁶² Turkish Accelerator Center Particle Factory Group, (A)Istinye University, 34010, Istanbul, Turkey; (B)Near East University, Nicosia, North Cyprus, 99138, Mersin 10, Turkey
- ⁶³ University of Bristol, (A)H H Wills Physics Laboratory; (B)Tyndall Avenue; (C)Bristol; (D)BS8 1TL
- ⁶⁴ University of Chinese Academy of Sciences, Beijing 100049, People's Republic of China
- ⁶⁵ University of Groningen, NL-9747 AA Groningen, The Netherlands
- ⁶⁶ University of Hawaii, Honolulu, Hawaii 96822, U.S.A.
- ⁶⁷ University of Jinan, Jinan 250022, People's Republic of China
- ⁶⁸ University of Manchester, Oxford Road, Manchester, M13 9PL, United Kingdom
- ⁶⁹ University of Muenster, Wilhelm-Klemm-Strasse 9, 48149 Muenster, Germany
- ⁷⁰ University of Oxford, Keble Road, Oxford OX13RH, United Kingdom
- ⁷¹ University of Science and Technology Liaoning, Anshan 114051, People's Republic of China
- ⁷² University of Science and Technology of China, Hefei 230026, People's Republic of China
- ⁷³ University of South China, Hengyang 421001, People's Republic of China
- ⁷⁴ University of the Punjab, Lahore-54590, Pakistan
- ⁷⁵ University of Turin and INFN, (A)University of Turin, I-10125, Turin, Italy; (B)University of Eastern Piedmont, I-15121, Alessandria, Italy; (C)INFN, I-10125, Turin, Italy
- ⁷⁶ Uppsala University, Box 516, SE-75120 Uppsala, Sweden
- ⁷⁷ Wuhan University, Wuhan 430072, People's Republic of China
- ⁷⁸ Yantai University, Yantai 264005, People's Republic of China
- ⁷⁹ Yunnan University, Kunming 650500, People's Republic of China
- ⁸⁰ Zhejiang University, Hangzhou 310027, People's Republic of China
- ⁸¹ Zhengzhou University, Zhengzhou 450001, People's Republic of China

^a Deceased

^b Also at the Moscow Institute of Physics and Technology, Moscow 141700, Russia

^c Also at the Novosibirsk State University, Novosibirsk, 630090, Russia

^d Also at the NRC "Kurchatov Institute", PNPI, 188300, Gatchina, Russia

^e Also at Goethe University Frankfurt, 60323 Frankfurt am Main, Germany

^f Also at Key Laboratory for Particle Physics, Astrophysics and Cosmology, Ministry of Education; Shanghai Key Laboratory for Particle Physics and Cosmology; Institute of Nuclear and Particle Physics, Shanghai 200240, People's Republic of China

^g Also at Key Laboratory of Nuclear Physics and Ion-beam Application (MOE) and Institute of Modern Physics, Fudan University, Shanghai 200443, People's Republic of China

^h Also at State Key Laboratory of Nuclear Physics and Technology, Peking University, Beijing 100871, People's Republic of China

ⁱ Also at School of Physics and Electronics, Hunan University, Changsha 410082, China

^j Also at Guangdong Provincial Key Laboratory of Nuclear Science, Institute of Quantum Matter, South China Normal University, Guangzhou 510006, China

^k Also at MOE Frontiers Science Center for Rare Isotopes, Lanzhou University, Lanzhou 730000, People's Republic of China

^l Also at Lanzhou Center for Theoretical Physics, Lanzhou University, Lanzhou 730000, People's Republic of China

^m Also at the Department of Mathematical Sciences, IBA, Karachi 75270, Pakistan

ⁿ Also at Ecole Polytechnique Federale de Lausanne (EPFL), CH-1015 Lausanne, Switzerland

^o Also at Helmholtz Institute Mainz, Staudinger Weg 18, D-55099 Mainz, Germany

^p Also at School of Physics, Beihang University, Beijing 100191, China